ACS ES&T Water

pubs.acs.org/estwater

Article

Nanopatterning Reduces Bacteria Fouling in Ultrafiltration

Lauren M. Ward,[§] Rushabh M. Shah,[§] Jessica D. Schiffman,* and Steven T. Weinman*

Cite This: https://doi.org/10.1021/acsestwater.2c00256

Read Online

ACCESS | Metrics & More | Article Recommendations

ABSTRACT: This contribution describes a method to reduce bacteria fouling on ultrafiltration membranes by applying nanoscale line-and-groove patterns on the surface of membranes. Nanoimprint lithography was used to pattern the polysulfone membrane surfaces with a peak height of 66.2 nm and a period of 594.0 nm. Surface characterization using scanning electron microscopy and atomic force microscopy confirmed that patterning was successful over the entire stamped area of the membrane. Water permeance tests determined that the permeance decreased by 36% upon patterning. Static batch experiments that explored the attachment of *Escherichia coli* K12 cells to the membranes demonstrated that the patterned membranes had a 60% lower attachment of microbes than the nonpatterned membranes. Dynamic bacteria fouling experiments using *E. coli* cells showed that the patterned membranes had a higher flux recovery ratio (88%) compared to the nonpatterned membranes (70%). On the basis of these studies, we suggest that patterning membranes can reduce the initial attachments of microbial cells and that different pattern sizes and shapes should be investigated to gain a fundamental understanding of their influence on bacteria fouling.

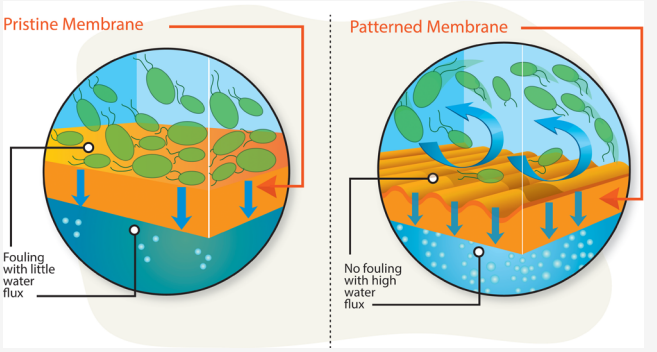

KEYWORDS: *patterned membrane, line-and-groove pattern, antifouling, ultrafiltration, nanoimprint lithography*

1. INTRODUCTION

Membranes are an integral technology for water and wastewater treatment. Specifically, pressure-driven membranes are used for a variety of applications, including turbidity removal (microfiltration, MF), bacteria and virus removal (ultrafiltration, UF), water softening (nanofiltration, NF), and seawater desalination (reverse osmosis, RO).[1] Also, UF membranes are commonly used to pretreat water before RO systems to prevent bacteria fouling of the RO membranes.[2,3] However, this leads to the UF membranes being susceptible to the foulants in the water.[3] One key foulant in many water types is bacteria. When bacteria foul a membrane, they often form a biofilm, resulting in an extreme reduction in membrane performance (i.e., lower rejection and water productivity).[4] Therefore, it is not surprising that bacteria fouling has been a well-studied topic in the literature.[5]

There have been numerous chemical modifications strategies used to prevent bacteria fouling.[6] One method is to modify the membranes with a hydrophilic coating that resists bacteria attachment, which are known as antifouling coatings.[7,8] Another method is to modify the membranes with polymers or agents that can kill the bacteria, which are known as antimicrobial or biocidal coatings.[9] Other strategies have used a combination of these two techniques to both resist bacteria fouling and kill the bacteria that do attach to prevent biofilm formation on the membrane.[10] For example, one study investigated the effect of TiO_2 nanopillars on *Pseudomonas aeruginosa* (*P. aeruginosa*) fouling for RO membrane applications. However, the TiO_2 also changed the surface chemistry of the membranes, so it is challenging to decouple the effect of the nanopillars' structure versus their chemistry.[11]

More recently, membrane patterning, ranging from the nanometer to millimeter scale, has been a technique studied to reduce numerous types of foulants,[12,13] including colloidal and particulates,[14,15] scaling and concentration polarization,[16,17] biopolymer and protein,[11,18−20] oil,[21] sludge,[22] as well as algae and yeast.[23] To the best of our knowledge, only three studies have investigated how bacteria fouling is affected by patterns on the surface of membranes.[24−26] Additionally, these studies are limited to investigating micron-sized patterns on poly(vinylidene fluoride) (PVDF) MF and polyamide RO membranes using only *P. aeruginosa* as the bacteria foulant.[24−26] None of these studies investigated the effect of surface patterning, specifically nanopatterns, on bacteria

Received: June 3, 2022
Revised: July 18, 2022
Accepted: July 28, 2022

fouling in UF, nor the effect of surface patterning when *Escherichia coli* K12 (*E. coli*) was used as the bacteria foulant.

The objective of this study was to test the hypothesis that line-and-groove nanopatterns on polysulfone (Psf) UF membranes would decrease *E. coli* fouling. *E. coli* was selected as the model bacteria foulant because it is commonly found in wastewater, and the detection of certain strains indicate fecal contamination.[27] In this work, we patterned a commercial Psf membrane with a nanoscale line-and-groove silicon stamp using thermal embossing. The patterned membranes were characterized and tested for pure water permeance, flux reduction, and flux recovery ratios, which is an indication of the membrane's resistance to fouling. Here, we demonstrate that line-and-groove nanopatterns hold potential to improve the fouling resistance and cleanability of patterned membranes compared to control UF membranes without surface patterns.

2. MATERIALS AND METHODS

2.1. Materials. Isopropyl alcohol (IPA, 70% v/v) was purchased from ThermoFisher Scientific (Waltham, MA). Deionized (DI) water was obtained from a Barnstead Nanopure Infinity water purification system (resistance of 18.2 MΩ cm, ThermoFisher Scientific). Phosphate-buffered saline (PBS, 1 × sterile biograde), Luria−Bertani broth (LB), M9 minimal salts (M9 media), sodium chloride (NaCl), D-(+)-glucose, and carbenicillin (BioReagent grade) were purchased from Sigma-Aldrich (St. Louis, MO). ACS reagent grade acetone was purchased from Fisher Scientific (Hampton, NH). Psf PS20 membranes were kindly provided by Solecta, Inc. (Oceanside, CA). All membrane samples came from the center portion of the roll to avoid any edge defects that might be present.

2.2. Membrane Patterning. Membranes were patterned with silicon line-and-groove stamps (29 mm × 12 mm) purchased from LightSmyth Technologies, Inc. (Eugene, OR). The stamps have a 606 nm period between the peaks, a 190 nm groove depth, and a 303 nm line width.[17,20,28] The membrane patterning procedure is consistent with our previous work.[17] Two stamps were placed side-by-side in contact with one another on top of the active layer of the Psf membrane. The membrane and stamps were placed on top of an 8 cm × 7.5 cm piece of 0.2 mm-thick aluminum shim (Grainger, Lake Forest, IL). A "cushion", which helped prevent the silicon stamps from breaking, of a 28.5 cm × 31 cm Kimwipe was folded to 1/16th its original size and placed on top of the membrane and stamps. Another similar size piece of the same aluminum shim was placed on top of the cushion and placed in an Auto C-PL, HC 3889 press from Carver, Inc. (Wabash, IN) to pattern the membrane. The press plates were heated to 45 °C and closed at a 25% pump speed until the pressure (force/stamp area) was 83.7 bar. The membrane was subject to this pressure for 15 min. The press did not hold a consistent pressure for the duration of the patterning process. The pressure slowly decreased to 69.7 bar before returning to the set pressure numerous times during the patterning time frame. The pressure would sometimes raise to 90.6 bar before returning to the set pressure.

2.3. Membrane Characterization. *2.3.1. Atomic Force Microscopy.* Atomic force microscopy (AFM) was utilized to observe the membrane surface before and after patterning after compaction from pure water permeance tests. The topography of the surface was characterized using a tapping mode AFM (Bruker NanoIR3, Billerica, MA). The tip used in the surface measurements possesses a spring constant k of ∼1−7 N/m with a resistance frequency of 75 ± 10 kHz, and the cantilever length was ∼225 μm. AFM images were taken with a 500 × 500 pixel resolution over 5 μm × 5 μm area at a scan rate of 0.5 Hz. The section analysis feature of the software (Gwyddion Version 2.61) was used to determine peak heights and root-mean-square (RMS) surface roughness.

2.3.2. Scanning Electron Microscopy. The morphology of the top surface of the membrane before and after patterning, as well as after compaction from pure water permeance tests was observed using a Thermo Fisher Apreo field-emission scanning electron microscope (FE-SEM) at The University of Alabama. Each membrane was attached to an aluminum stub with carbon tape and then gold coated prior to FE-SEM measurements. The FE-SEM measurements were performed at an accelerating voltage of 5.0 kV, a current voltage of 0.10 nA, and a magnification of 10,000×.

2.3.3. ATR-FTIR. Membrane chemistry before and after patterning was investigated using attenuated total reflectance Fourier transform infrared spectroscopy (ATR-FTIR). The membranes were rinsed in DI water, pat dried, and dried under a vacuum from ∼ −0.51 to −0.85 barg before analysis. The measurements were conducted using a PerkinElmer Spectrum 2 ATR-FTIR spectrometer equipped with a diamond ATR crystal in the range 4000-450 cm^{-1}. Data were processed by Spectrum 10 software. Each spectrum was collected for 128 scans at a resolution of 4 cm^{-1} and was baseline and ATR corrected with the Spectrum 10 software. All spectra were normalized to the peak at ∼1240 cm^{-1}. A background of the ATR crystal was taken before each set of samples was tested to ensure the crystal was clean.

2.3.4. Water Contact Angle. Static water contact angles were measured on both patterned and pristine membranes to evaluate the change in hydrophobicity caused by the patterns. The contact angles were collected with a Dataphysics OCA-15EC contact angle analyzer using the sessile drop method. A liquid drop of DI water (∼15 μL) was placed on the surface of each membrane. The SCA 20 Analysis software was used in the sessile drop model to determine the contact angle. Measurements were taken at ∼130 s after each drop was placed for consistency. A minimum of six measurements per membrane were taken to obtain an average contact angle measurement and standard deviation for each membrane type.

2.4. Membrane Performance Testing. *2.4.1. Pure Water Permeance.* A 10 mL dead-end stirred cell (Sterlitech, Kent, MA) with a membrane active area of 3.8 cm^2 was used to conduct pure water permeance experiments. First, a flushing procedure was conducted to remove the humectant from the pores of pristine and patterned Psf membranes. To flush the membranes, they were immersed in 70% IPA for 0.5 h, rinsed three times with DI water, and stored in DI water at 4 °C until use. The dead-end stirred cell was pressurized using a nitrogen (N_2) tank, and the flux was calculated by measuring the change of mass on the permeate side using a digital weighing scale (U.S. Solid, Cleveland, OH). Next, each flushed membrane was compacted for 0.5 h at 3 bar pressure to ensure that the flux change was less than 5%. Pure water flux tests were performed on the compacted membranes for 1 h at 1 bar transmembrane pressure (TMP). Experiments were conducted in triplicate for statistical relevance. Equation 1 was used to calculate permeance, which was equal to the volume of water that permeated through the membrane (ΔV) divided by the

https://doi.org/10.1021/acsestwater.2c00256
ACS EST Water XXXX, XXX, XXX−XXX

membrane footprint area (A) times the permeate collection time (Δt) times the transmembrane pressure (ΔP).

$$\text{permeance (L m}^{-2}\text{ h}^{-1}\text{ bar}^{-1}) = \frac{\Delta V}{A\Delta t\Delta P} \quad (1)$$

A custom-build cross-flow cell (channel dimensions of 28 mm long, 17 mm wide, and 1.5 mm deep, and an active area of 5.44 cm^2) equipped with 17 mil low-foulant spacer and a permeate carrier (Sterlitech),[29] was used to evaluate the pure water permeance of the pristine and patterned membranes. All tests were conducted at a flow rate of 50 mL min^{-1} enabled by a reciprocating pump (Eldex Laboratories Incorporated, Napa, CA) followed by a dampener (Cat Pumps, Minneapolis, MN).[30] A flushed pristine or patterned membrane (29 mm × 45 mm) was placed with its active side facing down into the cross-flow cell, where it was compacted for 0.5 h at a TMP of 4 bar. The desired TMP is calculated using the following equation:

$$\text{TMP (bar)} = \frac{P_{\text{feed}} + P_{\text{retentate}}}{2} - P_{\text{permeate}} \quad (2)$$

where P_{feed} is the pressure of the feed at the inlet of the flow cell, $P_{\text{retentate}}$ is the pressure of the retentate, and P_{permeate} is the pressure of the permeate. Post compaction, the pure water permeance was evaluated by applying a TMP of 1 bar for 1 h, using eq 1. The pure water tests were performed in triplicate for statistical relevance.

2.4.2. Static Bacteria Fouling. Static bacteria fouling tests were conducted as reported previously.[31] In brief, the Gram-negative bacterium *E. coli* K12 MG1655, containing a green fluorescent protein (GFP) plasmid, was purchased from DSMZ, Leibniz-Institut, Germany. Glass coverslips (22 mm × 22 mm, Fisher Scientific) were used as internal controls and were cleaned by submersion in an acetone bath (stirred at 60 rpm) for 10 min followed by rinsing with autoclaved DI water three times, before being dried at 60 °C for 16 h and treated with UV/ozone (ProCleanerTM, Bioforce Nanosciences, Ames, IA) for 10 min. Both sides of the pristine and patterned membranes (circular coupons, diameter = 2.54 cm) were sterilized for 10 min using a UV lamp (UVP UVGL-58, Analytik Jena US, Upland, CA). *E. coli* was inoculated with 100 μg mL^{-1} of carbenicillin and grown overnight in LB media at 37 °C to a concentration of 10^8 cells mL^{-1}. All membrane samples were placed at the base of six-well plates (Fisher Scientific) to which 5 mL of M9 media containing 250 μL of *E. coli* was added to each of the six wells and placed in an incubator at 37 °C for 2 h. Membranes were then removed from the six-well plates and lightly rinsed with M9 media to remove the loosely adherent bacteria. At least 15 random images of each sample were acquired using an Axio Imager A2M microscope (20× magnification, Zeiss, Thornwood, NY). Experiments were conducted in three parallel replicates on two different days for statistical relevance and biological replicates. Bacteria colony area coverage (%) was calculated using the particle analysis function in *ImageJ* 1.53a software,[32] consistent with our and others previous work.[8,33]

2.4.3. Dynamic Bacteria Fouling. Dynamic fouling experiments were performed on the membranes using the previously described dead-end stirred cell.[8,26,34,35] First, both sides of each membrane coupon were sterilized using the UV lamp for 10 min. *E. coli* were grown overnight in LB and resuspended in PBS (pH 7.4) to reach a concentration of 10^7 cells mL^{-1}. The initial pure water flux, $J_{w,i}$, was measured by passing DI water at 1 bar TMP for 1 h and determined using eq 3, where $\Delta V_{\text{DIwater}}$ is the volume of water that permeated through the membrane, Δt is the time, and A is the membrane area.

$$J_{w,i}\ (\text{L m}^{-2}\text{ h}^{-1}) = \frac{\Delta V_{\text{DIwater}}}{A\Delta t} \quad (3)$$

$$J_{E.coli}\ (\text{L m}^{-2}\text{ h}^{-1}) = \frac{\Delta V_{E.coli}}{A\Delta t} \quad (4)$$

$$J_{w,f}\ (\text{L m}^{-2}\text{ h}^{-1}) = \frac{\Delta V_{\text{DIwater}}}{A\Delta t} \quad (5)$$

$$\text{FRR (\%)} = \frac{J_{w,f}}{J_{w,i}} \times 100 \quad (6)$$

The fouling experiment was carried out by passing 40 mL of the bacteria suspensions at 1 bar TMP with a stir rate of 600 rpm to find the flux rate, $J_{E.\ coli}$ (eq 4).[8,36] Following *E. coli* filtration, the membrane coupons were rinsed with PBS for 10 min, and the final pure water flux, $J_{w,f}$, was measured (eq 5).[35] The flux recovery ratios (FRRs) were calculated using eq 6 and are the ratio of final pure water flux and initial pure water flux of the membranes. All the dynamic fouling experiments were performed in triplicate for statistical relevance.

2.5. Statistics. For all of the data, an unpaired Student's t test was conducted in Microsoft Excel (Version 2203) to determine the statistically significant difference between samples. Significance is denoted in the graphs using asterisks (*) and defined in figure captions.

3. RESULTS AND DISCUSSION

3.1. Surface Patterning. The PS20 membranes were patterned directly with silicon stamps by thermal embossing. This causes the membrane to deform and mold into the pattern shape, such that the pattern on the membrane will be a negative of the stamp pattern.[14,17,20,28] Figures 1 and 2 show the changes to the surface that happens during the patterning process. Figure 1 shows the SEM images taken of the membrane. A noticeable line-and-groove pattern is visible in the patterned membrane in Figure 1B. There does not seem to be any noticeable difference for both the patterned and pristine

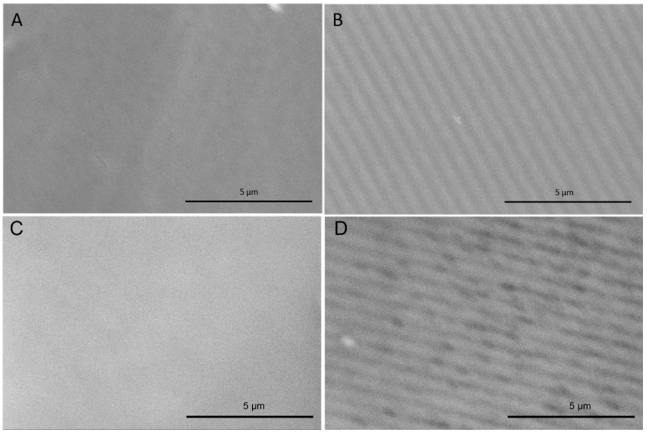

Figure 1. SEM images of a (A) pristine PS20 membrane before compaction, (B) patterned PS20 membrane before compaction, (C) pristine PS20 membrane after compaction, and (D) patterned PS20 membrane after compaction. The images were taken at 10,000× magnification, and the common scale bar is 5 μm.

https://doi.org/10.1021/acsestwater.2c00256
ACS EST Water XXXX, XXX, XXX−XXX

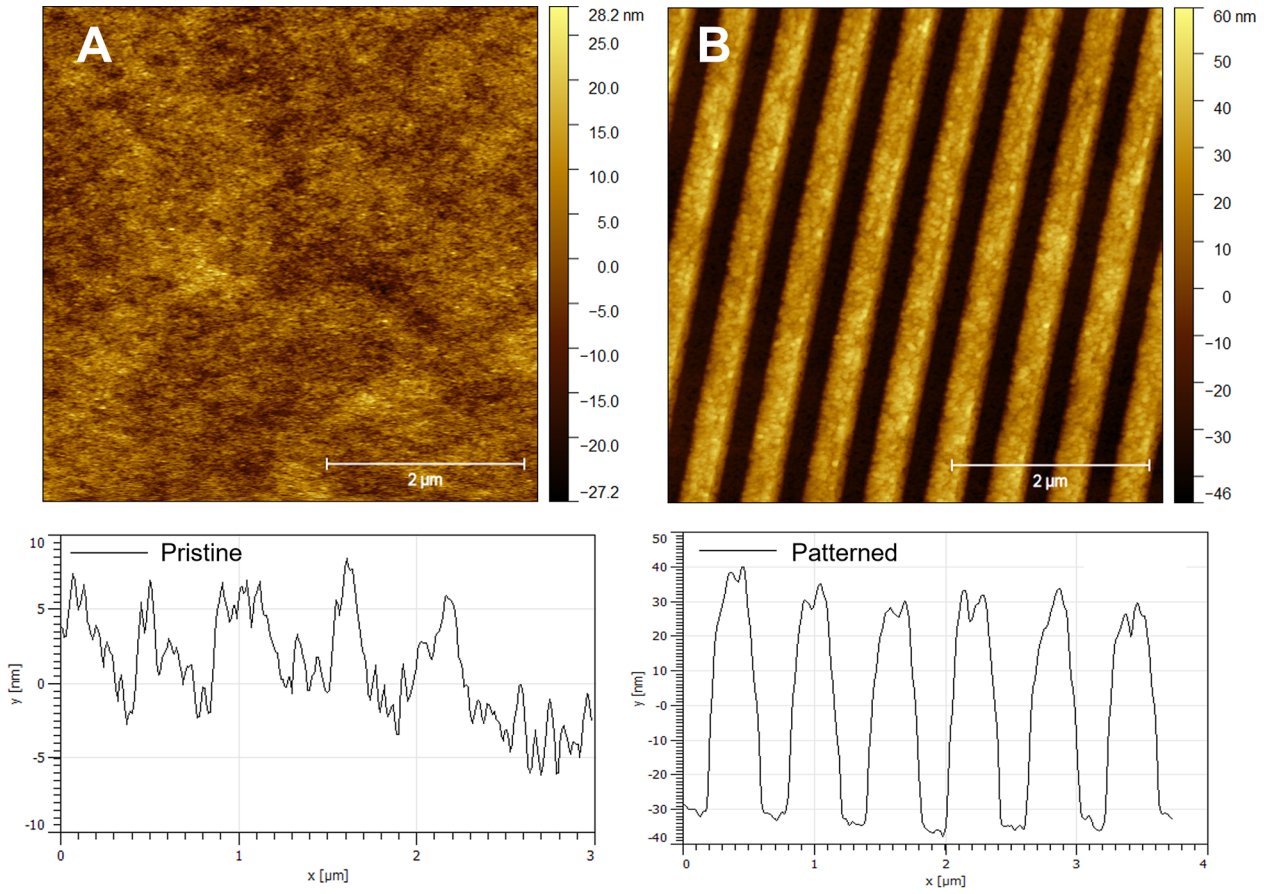

Figure 2. AFM images and cross-sectional profiles of (A) pristine and (B) patterned PS20 membranes after compaction. The common scan area is 5 μm × 5 μm.

membranes after compaction at 3 bar, as can be seen in Figure 1C,D. *ImageJ* was used to determine the peak-to-peak distance on the patterned membranes in Figure 1B,D. The distances were 595 ± 2 and 581 ± 1 nm for the compacted and prior to compacted membranes, respectively. These peak-to-peak distances are not statistically different at p = 0.05 (n = 15). Because there is not a significant difference between the peak-to-peak distances before and after compaction, AFM images were taken only after compaction.

Figure 2 shows the AFM images of the pristine and patterned membrane after compaction, along with a cross-sectional profile of each image. Figure 2B shows the clear patterns that were embossed into the membrane. The peak height of the pattern was determined to be 66.2 ± 3.8 nm using the AFM sectional analysis tool. Our average peak height is lower than the average peak height that was previously reported to of 179 nm by Weinman et al. when the same stamp was applied to a similar membrane (Nanostone is now Solecta).[28] This is likely due to a lower patterning pressure being used in this study (83.7 bar) compared to their study (189 bar) due to a greater area being stamped. The period of the pattern (peak-to-peak distance) was determined to be 594.0 ± 66.7 nm, which is comparable to other studies using this stamp.[20,28] On the basis of the pattern dimensions, it was calculated that the patterned membranes had a 29.4% increase in surface area, with the pristine membranes having a 6.4 cm^2 surface area and the patterned membranes having an 8.3 cm^2 surface area. The z-scale on the side of each image represents the height of the topography of the membrane surface. The pristine membrane in Figure 2A has a smaller scale due to there being less variance of the height. In Figure 2B, the scale is larger due to there being a larger difference from the top of the pattern to the lowest point. This difference also causes the difference in the height scale on the cross-sectional profiles. Table 1 shows the RMS surface roughness data from the AFM images of the membranes after compaction. As expected, the RMS roughness was higher for the patterned membranes compared to the pristine membranes. However, when the RMS roughness was analyzed for only the peaks and the valleys of the patterns, the peaks were found to be statistically similar (p = 0.05) to the pristine membranes at 3.6 ± 0.3 nm and the valleys were found to be statistically similar (p = 0.05) to the pristine membranes at 2.4 ± 0.6 nm. While ordered roughness has been added to the membrane in the form of patterns, the roughness of the membrane surface itself has not been altered.

Table 1. Pristine and Patterned PS20 Membrane Characteristics[a]

membrane	water contact angle (°)	RMS surface roughness after compaction (nm)
pristine	89.2 ± 2.6	3.4 ± 0.2
patterned	84.9 ± 3.7	6.1 ± 0.7

[a]Water contact angle error represents one standard deviation from six samples. Surface roughness error represents one standard deviation from three samples.

Table 1 also shows the water contact angle data of the pristine and patterned PS20 membranes. The water contact

https://doi.org/10.1021/acsestwater.2c00256
ACS EST Water XXXX, XXX, XXX−XXX

angle for the patterned PS20 membrane is slightly statistically lower ($p = 0.05$) than that of the pristine membrane, indicating a transition to the Wenzel wetting state,[37] which is common for patterning hydrophilic (<90° water contact angle) surfaces.

Figure 3 shows the ATR-FTIR spectra of the pristine and patterned membranes. The spectra are overlapping, indicating

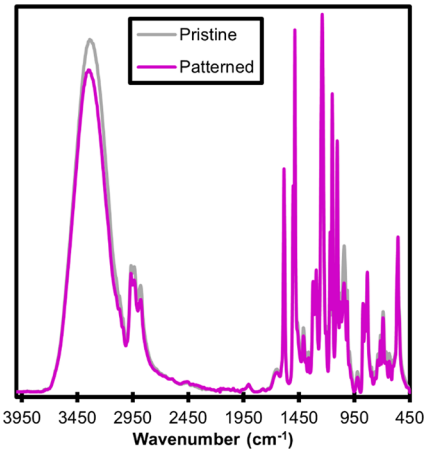

Figure 3. ATR-FTIR spectra of a pristine and patterned PS20 membrane. Spectra are normalized to the peak at 1240 cm^{-1}.

no change in the functional groups of the membrane before and after patterning, as expected. The peaks at ~1590, ~1505, ~1490, ~1325, ~1295, ~1240, ~1170, ~1150, and ~835 cm^{-1} are typical of Psf membranes.[28,38] The large peak in the 3340 cm^{-1} region is indicative of − OH bonds, and the peaks at ~2940 and ~2880 cm^{-1} are indicative of $-CH_2-$ bonds, suggesting this membrane is coated, likely with a polymer, like poly(vinyl alcohol),[38,39] to help reduce membrane fouling. These results combined with the surface roughness and water contact angle data imply that any changes seen in membrane performance are due to patterns on the membrane surface and not any changes to the surface chemistry or roughness of the membrane surface.

3.2. Membrane Performance. *3.2.1. Pure Water Permeance.* Next, we measured the pure water permeance of pristine PS20 membranes and patterned PS20 membranes using the dead-end stirred cell. The permeance values reported in Figure 4A are the mean values over 1 h of filtration at the steady-state condition, i.e., post compaction. The pristine PS20 membranes had an average pure water permeance of ~35 L m^{-2} h^{-1} bar^{-1}. The patterned PS20 membranes had a statistically lower pure water permeance of ~22 L m^{-2} h^{-1} bar^{-1}. One would expect that, by calculating the water permeance using footprint area, the water permeance for the patterned membrane should increase due to the increase in available surface area for permeation. Potentially, this permeance reduction could be attributed to pore size reduction or collapse due to the pressure applied during stamping, as observed in other reports.[14,28,40]

The cross-flow pure water permeance of the pristine PS20 and patterned PS20 membranes were determined at a TMP of 1 bar, postcompacting the membranes at 4 bar (see Figure 4B). The direction of flow was perpendicular (i.e., 90°) to the patterned lines. The patterned PS20 membranes exhibited a statistically lower permeance than the pristine PS20 membranes. The pure water permeance for pristine PS20 and patterned PS20 were 241 ± 67 and 157 ± 21 L m^{-2} h^{-1} bar^{-1}, respectively. These results further support the fact that some pores collapse on applying high pressure during the stamping process.[14,28,40] Even after applying high pressure during stamping, the decrease in the permeance was only ~35%. The differences between the dead-end and cross-flow results are likely due to a number of factors, such as the difference in the hydraulic resistance of the membrane supporting base plates and the difference in the shear stress in the two systems.[41]

3.2.2. Static Resistance to Bacteria Fouling. The resistance to bacterial fouling was determined for the pristine PS20 and patterned PS20 membranes using a static assay featuring the model microorganism *E. coli*. Figure 5 shows that statistically fewer *E. coli* attached to the patterned PS20 than to the pristine PS20 membranes after a 2 h incubation period. In comparison to the pristine PS20 membranes, *E. coli* attachment decreased by more than 60%, to 38 ± 8% for patterned PS20 membranes. Glass coverslips (run as internal control) fouled significantly more than both pristine PS20 and patterned PS20 membranes (data not shown). Our results demonstrate that patterned PS20 membranes are highly repellant to *E. coli*. The line-and-groove nanopatterns potentially reduce the bacteria-membrane contact, thus improving the bacterial antifouling capabilities of patterned PS20 membranes. Previous studies have demon-

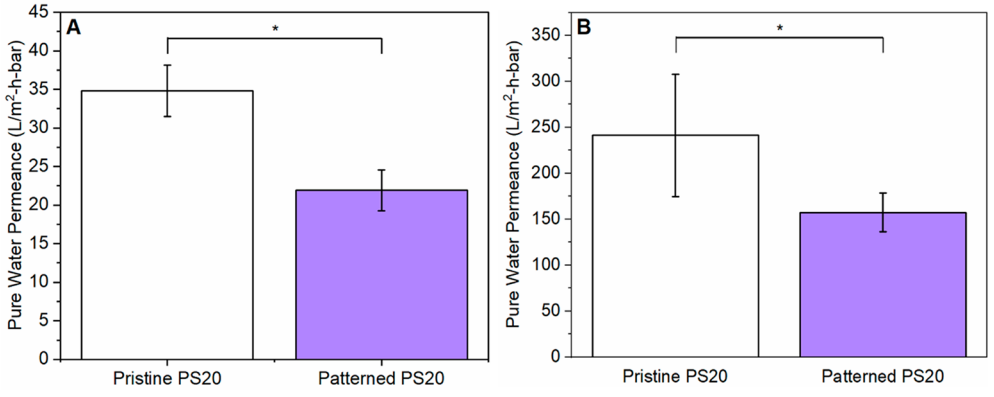

Figure 4. (A) Dead-end pure water permeance of pristine PS20 and patterned PS20 membranes at 1 bar TMP. (B) Cross-flow pure water permeance of pristine PS20 and patterned PS20 membranes at 1 bar TMP. Error bars denote one standard deviation; one asterisk (*) denotes a $p \leq 0.05$ significance between samples.

https://doi.org/10.1021/acsestwater.2c00256
ACS EST Water XXXX, XXX, XXX−XXX

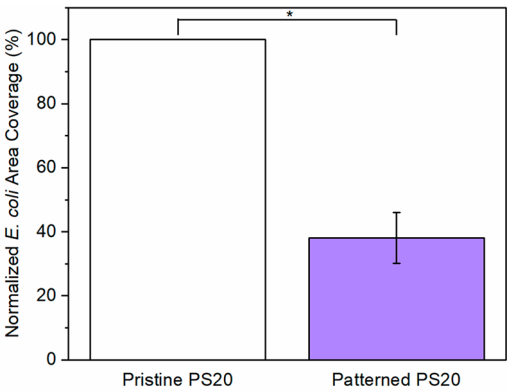

Figure 5. Normalized *E. coli* area coverage after 2 h of incubation on pristine PS20 and patterned PS20 membranes. Error bars denote one standard deviation; one asterisk (*) denotes a $p \leq 0.01$ significance between samples.

strated that nanotopography decreases the contact area between a polymer substrate and bacteria in a static assay.[42]

3.2.3. Dynamic Bacteria Fouling Resistance. The dynamic resistance to *E. coli* fouling of the pristine PS20 and patterned PS20 membranes were evaluated using the dead-end stirred cell using bacteria suspensions. Initial fluxes of pristine PS20 and patterned PS20 were statistically equivalent at 112 ± 14 and 111 ± 10 L m^{-2} h^{-1}, respectively. As shown in Figure 6A, the initial flux of both the pristine PS20 and patterned PS20 membrane decreased sharply since the bacteria instantaneously deposited on the membrane surface. It can be observed that, after 10 min of rinsing with PBS solution, the patterned PS20 membranes demonstrated a larger flux recovery compared to the pristine PS20 membranes. In comparison to the pristine PS20 membranes, Figure 6B shows that the patterned PS20 membranes had a statistical increase in their FRR, which is a measure of the dynamic fouling resistance of a membrane. The FRR increased from 70 ± 1% for pristine PS20 membranes to 88 ± 3% for the patterned PS20 membranes when challenged using a high concentration of *E. coli* (10^7 CFU mL^{-1}). Previous studies wherein the FRR was tested using *P. aeruginosa* (10^4–10^6 CFU mL^{-1})[11,24] or bovine serum albumin (BSA) (1 g L^{-1})[12] on different patterned membrane types showed similar FRR trends. *E. coli* is a rod-shaped bacteria that is generally 0.5 μm in diameter by one micron in length. The patterns are ~0.07 μm in height and ~0.6 μm in peak-to-peak distance. This size would allow for the *E. coli* to deposit into the pattern only if it is aligned parallel (0°) to the pattern but likely not deposit all the way down into the valley. This would likely lead to an enhanced flux recovery after rinsing.[19] If the *E. coli* tried to deposit perpendicular (90°) to the patterns or at another angle that is not parallel to the pattern, then the contact area between the bacteria and the membranes would be reduced compared to the flat membrane, leading to less overall fouling.[14,29,42,43] Thus, our results suggest that *E. coli* deposited more parallel to the patterns due to the enhanced flux recovery and little difference in flux decline.

4. CONCLUSION

Nanoimprint lithography was used to pattern a commercial ultrafiltration membrane to reduce membrane bacteria fouling as demonstrated in this work using *E. coli* K12. Nanopatterned membranes reduced static bacteria attachment by over 60%. Dynamic fouling experiments show that the nanopatterned membranes had an improved FRR of 88% compared to the pristine membranes, which had a FRR of 70%. The enhanced static fouling resistance was attributed to a decrease in bacteria-membrane contact. The improved cleanability was attributed to the *E. coli* not being able to deposit down in the valleys of the patterns. These results supported our hypothesis that the nanopatterns improved *E. coli* fouling resistance. That being said, the rate of fouling was similar for both the nanopatterned and pristine membranes. Ongoing work is exploring other pattern sizes and shapes to further improve static bacteria attachment and flux recovery and to reduce the rate of fouling on the pattern membranes compared to pristine membranes.

AUTHOR INFORMATION

Corresponding Authors

Jessica D. Schiffman − *Department of Chemical Engineering, University of Massachusetts Amherst, Amherst, Massachusetts 01003, United States;* orcid.org/0000-0002-1265-5392; Phone: +1 (413) 545-6143; Email: schiffman@umass.edu

Steven T. Weinman − *Department of Chemical and Biological Engineering, The University of Alabama, Tuscaloosa, Alabama 35487, United States;* orcid.org/0000-0001-9911-0119; Phone: +1 (205) 348-8516; Email: stweinman@eng.ua.edu

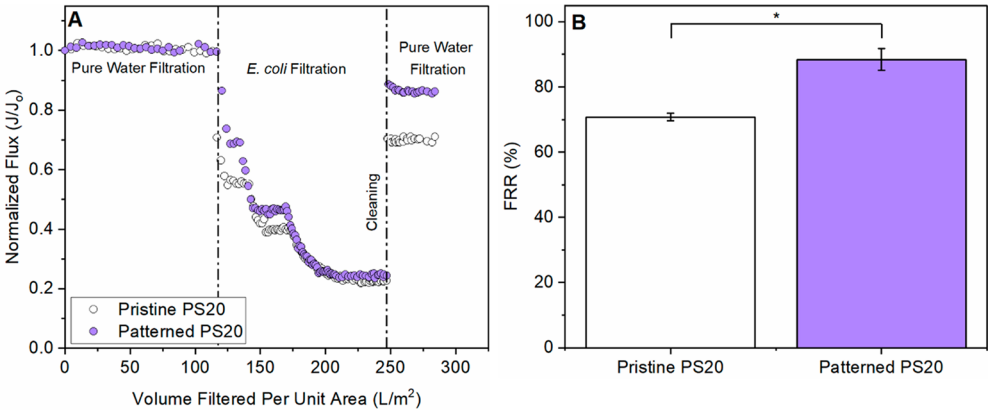

Figure 6. (A) Flux decline and recovery of the pristine PS20 and patterned PS20 membranes during *E. coli* filtration and after membrane cleaning. (B) Flux recovery ratio (FRR) of pristine PS20 and patterned PS20 membranes. Error bars denote one standard deviation; one asterisk (*) denotes a $p \leq 0.05$ significance between samples.

https://doi.org/10.1021/acsestwater.2c00256
ACS EST Water XXXX, XXX, XXX−XXX

Authors

Lauren M. Ward − *Department of Chemical and Biological Engineering, The University of Alabama, Tuscaloosa, Alabama 35487, United States*

Rushabh M. Shah − *Department of Chemical Engineering, University of Massachusetts Amherst, Amherst, Massachusetts 01003, United States;* orcid.org/0000-0002-1812-3717

Complete contact information is available at: https://pubs.acs.org/10.1021/acsestwater.2c00256

Author Contributions

§L.M.W. and R.M.S. contributed equally to this work. CRediT: **Lauren M. Ward** conceptualization (equal), data curation (equal), formal analysis (equal), funding acquisition (supporting), investigation (equal), methodology (equal), visualization (equal), writing-original draft (equal), writing-review & editing (equal); **Rushabh M. Shah** conceptualization (equal), data curation (equal), formal analysis (equal), funding acquisition (supporting), investigation (equal), methodology (equal), visualization (equal), writing-original draft (equal), writing-review & editing (equal); **Jessica D. Schiffman** conceptualization (equal), formal analysis (equal), funding acquisition (equal), methodology (equal), project administration (equal), resources (equal), supervision (equal), validation (equal), writing-original draft (supporting), writing-review & editing (equal); **Steven T. Weinman** conceptualization (equal), formal analysis (equal), funding acquisition (equal), investigation (equal), project administration (equal), resources (equal), supervision (equal), validation (equal), writing-original draft (supporting), writing-review & editing (equal).

Notes

The authors declare no competing financial interest.

■ ACKNOWLEDGMENTS

L.M.W. was supported by a GAANN Fellowship from the United States Department of Education (DoEd) under award number P200A189956. The authors wish to acknowledge the National Science Foundation (NSF) for financial support under NSF award numbers CBET-1941700 and CBET-1930610. R.M.S. thanks the American Membrane Technology Association (AMTA) and United States Bureau of Reclamation for the Fellowship in Membrane Technology. Any opinions, findings, conclusions, and/or recommendations expressed in this material are those of the author(s) and do not necessarily reflect the views of the DoEd and NSF. The authors thank Solecta, Inc. for kindly provided the membranes used in this study. The authors thank Prof. Ayanjeet Ghosh and Md Hasan Ul Iqbal at The University of Alabama for their help with the AFM measurements and analysis. The authors thank Xiao Han for their help with preliminary AFM measurements and analysis.

■ REFERENCES

(1) Anis, S. F.; Hashaikeh, R.; Hilal, N. Microfiltration membrane processes: A review of research trends over the past decade. *Journal of Water Process Engineering* **2019**, *32*, 100941. Al Aani, S.; Mustafa, T. N.; Hilal, N. Ultrafiltration membranes for wastewater and water process engineering: A comprehensive statistical review over the past decade. *Journal of Water Process Engineering* **2020**, *35*, 101241. Yang, Z.; Zhou, Y.; Feng, Z.; Rui, X.; Zhang, T.; Zhang, Z. A review on reverse osmosis and nanofiltration membranes for water purification. *Polymers* **2019**, *11* (8), 1252.

(2) Pearce, G. K. UF/MF pre-treatment to RO in seawater and wastewater reuse applications: a comparison of energy costs. *Desalination* **2008**, *222* (1), 66−73.

(3) Brover, S.; Lester, Y.; Brenner, A.; Sahar-Hadar, E. Optimization of ultrafiltration as pre-treatment for seawater RO desalination. *Desalination* **2022**, *524*, 115478.

(4) Herzberg, M.; Elimelech, M. Biofouling of reverse osmosis membranes: role of biofilm-enhanced osmotic pressure. *J. Membr. Sci.* **2007**, *295* (1), 11−20.

(5) Pichardo-Romero, D.; Garcia-Arce, Z. P.; Zavala-Ramírez, A.; Castro-Muñoz, R. Current advances in biofouling mitigation in membranes for water treatment: An Overview. *Processes* **2020**, *8* (2), 182.

(6) Rana, D.; Matsuura, T. Surface modifications for antifouling membranes. *Chem. Rev.* **2010**, *110* (4), 2448−2471.

(7) Hadidi, M.; Zydney, A. L. Fouling behavior of zwitterionic membranes: Impact of electrostatic and hydrophobic interactions. *J. Membr. Sci.* **2014**, *452*, 97−103. Kang, G.-d.; Cao, Y.-m. Development of antifouling reverse osmosis membranes for water treatment: a review. *Water Res.* **2012**, *46* (3), 584−600. Kochkodan, V.; Hilal, N. A comprehensive review on surface modified polymer membranes for biofouling mitigation. *Desalination* **2015**, *356*, 187−207. Shahkaramipour, N.; Jafari, A.; Tran, T.; Stafford, C. M.; Cheng, C.; Lin, H. Maximizing the grafting of zwitterions onto the surface of ultrafiltration membranes to improve antifouling properties. *J. Membr. Sci.* **2020**, *601*, 117909. Wardrip, N. C.; Dsouza, M.; Urgun-Demirtas, M.; Snyder, S. W.; Gilbert, J. A.; Arnusch, C. J. Printing-assisted surface modifications of patterned ultrafiltration membranes. *ACS Appl. Mater. Interfaces* **2016**, *8* (44), 30271−30280.

(8) Dobosz, K. M.; Kuo-LeBlanc, C. A.; Emrick, T.; Schiffman, J. D. Antifouling ultrafiltration membranes with retained pore size by controlled deposition of zwitterionic polymers and poly(ethylene glycol). *Langmuir* **2019**, *35* (5), 1872−1881.

(9) Tiller, J. C.; Liao, C.-J.; Lewis, K.; Klibanov, A. M. Designing surfaces that kill bacteria on contact. *Proc. Natl. Acad. Sci. U. S. A.* **2001**, *98* (11), 5981−5985. Perreault, F. o.; Tousley, M. E.; Elimelech, M. Thin-film composite polyamide membranes functionalized with biocidal graphene oxide nanosheets. *Environ. Sci. Technol. Lett.* **2014**, *1* (1), 71−76. Tiraferri, A.; Vecitis, C. D.; Elimelech, M. Covalent binding of single-walled carbon nanotubes to polyamide membranes for antimicrobial surface properties. *ACS Appl. Mater. Interfaces* **2011**, *3* (8), 2869−2877. Li, W.-R.; Xie, X.-B.; Shi, Q.-S.; Zeng, H.-Y.; You-Sheng, O.-Y.; Chen, Y.-B. Antibacterial activity and mechanism of silver nanoparticles on Escherichia coli. *Appl. Microbiol. Biotechnol.* **2010**, *85* (4), 1115−1122. Zhu, J.; Hou, J.; Zhang, Y.; Tian, M.; He, T.; Liu, J.; Chen, V. Polymeric antimicrobial membranes enabled by nanomaterials for water treatment. *J. Membr. Sci.* **2018**, *550*, 173−197.

(10) Weinman, S. T.; Bass, M.; Pandit, S.; Herzberg, M.; Freger, V.; Husson, S. M. A switchable zwitterionic membrane surface chemistry for biofouling control. *J. Membr. Sci.* **2018**, *548*, 490−501. Mi, L.; Jiang, S. Integrated antimicrobial and nonfouling zwitterionic polymers. *Angew. Chem., Int. Ed.* **2014**, *53* (7), 1746−1754. Sawada, I.; Fachrul, R.; Ito, T.; Ohmukai, Y.; Maruyama, T.; Matsuyama, H. Development of a hydrophilic polymer membrane containing silver nanoparticles with both organic antifouling and antibacterial properties. *J. Membr. Sci.* **2012**, *387*, 1−6. Nisola, G. M.; Park, J. S.; Beltran, A. B.; Chung, W.-J. Silver nanoparticles in a polyether-block-polyamide copolymer towards antimicrobial and antifouling membranes. *RSC Adv.* **2012**, *2* (6), 2439−2448. Zou, P.; Hartleb, W.; Lienkamp, K. It takes walls and knights to defend a castle−synthesis of surface coatings from antimicrobial and antibiofouling polymers. *J. Mater. Chem.* **2012**, *22* (37), 19579−19589. Yu, Q.; Cho, J.; Shivapooja, P.; Ista, L. K.; López, G. P. Nanopatterned smart polymer surfaces for controlled attachment, killing, and release of bacteria. *ACS Appl. Mater. Interfaces* **2013**, *5* (19), 9295−9304. Ren, L.; Chen, J.; Lu, Q.; Han, J.; Wu, H. Anti-biofouling nanofiltration membrane constructed by in-situ photo-grafting bactericidal and hydrophilic polymers. *J. Membr. Sci.* **2021**, *617*, 118658.

(11) Choi, W.; Chan, E. P.; Park, J.-H.; Ahn, W.-G.; Jung, H. W.; Hong, S.; Lee, J. S.; Han, J.-Y.; Park, S.; Ko, D.-H.; et al. Nanoscale pillar-enhanced tribological surfaces as antifouling membranes. *ACS Appl. Mater. Interfaces* **2016**, *8* (45), 31433−31441.
(12) Ding, Y.; Maruf, S.; Aghajani, M.; Greenberg, A. R. Surface patterning of polymeric membranes and its effect on antifouling characteristics. *Sep. Sci. Technol.* **2017**, *52* (2), 240−257.
(13) Heinz, O.; Aghajani, M.; Greenberg, A. R.; Ding, Y. Surface-patterning of polymeric membranes: fabrication and performance. *Current Opinion in Chemical Engineering* **2018**, *20*, 1−12. Barambu, U. N.; Bilad, R. M.; Wibisono, Y.; Jaafar, J.; Mahlia, M. T.; Khan, L. A. Membrane surface patterning as a fouling mitigation strategy in liquid filtration: A review. *Polymers* **2019**, *11* (10), 1687.
(14) Maruf, S. H.; Wang, L.; Greenberg, A. R.; Pellegrino, J.; Ding, Y. Use of nanoimprinted surface patterns to mitigate colloidal deposition on ultrafiltration membranes. *J. Membr. Sci.* **2013**, *428*, 598−607.
(15) Maruf, S. H.; Greenberg, A. R.; Pellegrino, J.; Ding, Y. Critical flux of surface-patterned ultrafiltration membranes during cross-flow filtration of colloidal particles. *J. Membr. Sci.* **2014**, *471*, 65−71. Jang, J. H.; Lee, J.; Jung, S.-Y.; Choi, D.-C.; Won, Y.-J.; Ahn, K. H.; Park, P.-K.; Lee, C.-H. Correlation between particle deposition and the size ratio of particles to patterns in nano-and micro-patterned membrane filtration systems. *Sep. Purif. Technol.* **2015**, *156*, 608−616. Won, Y.-J.; Jung, S.-Y.; Jang, J.-H.; Lee, J.-W.; Chae, H.-R.; Choi, D.-C.; Ahn, K. H.; Lee, C.-H.; Park, P.-K. Correlation of membrane fouling with topography of patterned membranes for water treatment. *J. Membr. Sci.* **2016**, *498*, 14−19. Choi, D.-C.; Jung, S.-Y.; Won, Y.-J.; Jang, J. H.; Lee, J.-W.; Chae, H.-R.; Lim, J.; Ahn, K. H.; Lee, S.; Kim, J.-H.; et al. Effect of pattern shape on the initial deposition of particles in the aqueous phase on patterned membranes during crossflow filtration. *Environ. Sci. Technol. Lett.* **2017**, *4* (2), 66−70. Jung, S. Y.; Ahn, K. H. Transport and deposition of colloidal particles on a patterned membrane surface: Effect of cross-flow velocity and the size ratio of particle to surface pattern. *J. Membr. Sci.* **2019**, *572*, 309−319. Malakian, A.; Husson, S. M. Understanding the roles of patterning and foulant chemistry on nanofiltration threshold flux. *J. Membr. Sci.* **2020**, *597*, 117746. ElSherbiny, M. I.; Khalil, S. A.; Ulbricht, M. Influence of surface micro-patterning and hydrogel coating on colloidal silica fouling of polyamide thin-film composite membranes. *Membranes* **2019**, *9* (6), 67.
(16) Maruf, S. H.; Greenberg, A. R.; Pellegrino, J.; Ding, Y. Fabrication and characterization of a surface-patterned thin film composite membrane. *J. Membr. Sci.* **2014**, *452*, 11−19. Zhou, Z.; Ling, B.; Battiato, I.; Husson, S. M.; Ladner, D. A. Concentration polarization over reverse osmosis membranes with engineered surface features. *J. Membr. Sci.* **2021**, *617*, 118199.
(17) Ward, L. M.; Fickling, B. G.; Weinman, S. T. Effect of nanopatterning on concentration polarization during nanofiltration. *Membranes* **2021**, *11* (12), 961.
(18) Maruf, S. H.; Rickman, M.; Wang, L.; Mersch, J., IV; Greenberg, A. R.; Pellegrino, J.; Ding, Y. Influence of sub-micron surface patterns on the deposition of model proteins during active filtration. *J. Membr. Sci.* **2013**, *444*, 420−428. Rickman, M.; Maruf, S.; Kujundzic, E.; Davis, R. H.; Greenberg, A.; Ding, Y.; Pellegrino, J. Fractionation and flux decline studies of surface-patterned nanofiltration membranes using NaCl-glycerol-BSA solutions. *J. Membr. Sci.* **2017**, *527*, 102−110. Xie, M.; Luo, W.; Gray, S. R. Surface pattern by nanoimprint for membrane fouling mitigation: Design, performance and mechanisms. *Water Res.* **2017**, *124*, 238−243. Mazinani, S.; Al-Shimmery, A.; Chew, Y. M. J.; Mattia, D. 3D printed fouling-resistant composite membranes. *ACS Appl. Mater. Interfaces* **2019**, *11* (29), 26373−26383. Asad, A.; Sadrzadeh, M.; Sameoto, D. Direct micropatterning of phase separation membranes using hydrogel soft lithography. *Advanced Materials Technologies* **2019**, *4* (7), 1800384.
(19) Gohari, R. J.; Lau, W. J.; Matsuura, T.; Ismail, A. F. Effect of surface pattern formation on membrane fouling and its control in phase inversion process. *J. Membr. Sci.* **2013**, *446*, 326−331.
(20) Weinman, S. T.; Husson, S. M. Influence of chemical coating combined with nanopatterning on alginate fouling during nanofiltration. *J. Membr. Sci.* **2016**, *513*, 146−154.
(21) Al-Shimmery, A.; Mazinani, S.; Ji, J.; Chew, Y. M. J.; Mattia, D. 3D printed composite membranes with enhanced anti-fouling behaviour. *J. Membr. Sci.* **2019**, *574*, 76−85. Kharraz, J. A.; Farid, M. U.; Khanzada, N. K.; Deka, B. J.; Arafat, H. A.; An, A. K. Macro-corrugated and nano-patterned hierarchically structured super-omniphobic membrane for treatment of low surface tension oily wastewater by membrane distillation. *Water Res.* **2020**, *174*, 115600.
(22) Won, Y.-J.; Lee, J.; Choi, D.-C.; Chae, H. R.; Kim, I.; Lee, C.-H.; Kim, I.-C. Preparation and application of patterned membranes for wastewater treatment. *Environ. Sci. Technol.* **2012**, *46* (20), 11021−11027. Lyu, Z.; Ng, T. C. A.; Tran-Duc, T.; Lim, G. J. H.; Gu, Q.; Zhang, L.; Zhang, Z.; Ding, J.; Phan-Thien, N.; Wang, J.; et al. 3D-printed surface-patterned ceramic membrane with enhanced performance in crossflow filtration. *J. Membr. Sci.* **2020**, *606*, 118138. Osman, A.; Mat Nawi, I. N.; Samsuri, S.; Bilad, R. M.; Shamsuddin, N.; Khan, L. A.; Jaafar, J.; Nordin, A. N. Patterned membrane in an energy-efficient tilted panel filtration system for fouling control in activated sludge filtration. *Polymers* **2020**, *12* (2), 432.
(23) Gençal, Y.; Durmaz, E.; Çulfaz-Emecen, P. Preparation of patterned microfiltration membranes and their performance in crossflow yeast filtration. *J. Membr. Sci.* **2015**, *476*, 224−233. Zhao, Z.; Ilyas, A.; Muylaert, K.; Vankelecom, I. F. J. Optimization of patterned polysulfone membranes for microalgae harvesting. *Bioresour. Technol.* **2020**, *309*, 123367.
(24) Won, Y.-J.; Choi, D.-C.; Jang, J. H.; Lee, J.-W.; Chae, H. R.; Kim, I.; Ahn, K. H.; Lee, C.-H.; Kim, I.-C. Factors affecting pattern fidelity and performance of a patterned membrane. *J. Membr. Sci.* **2014**, *462*, 1−8.
(25) Choi, W.; Lee, C.; Lee, D.; Won, Y. J.; Lee, G. W.; Shin, M. G.; Chun, B.; Kim, T.-S.; Park, H.-D.; Jung, H. W.; et al. Sharkskin-mimetic desalination membranes with ultralow biofouling. *Journal of Materials Chemistry A* **2018**, *6* (45), 23034−23045.
(26) Choi, W.; Lee, C.; Yoo, C. H.; Shin, M. G.; Lee, G. W.; Kim, T.-S.; Jung, H. W.; Lee, J. S.; Lee, J.-H. Structural tailoring of sharkskin-mimetic patterned reverse osmosis membranes for optimizing biofouling resistance. *J. Membr. Sci.* **2020**, *595*, 117602.
(27) Frigon, D.; Biswal, B. K.; Mazza, A.; Masson, L.; Gehr, R. Biological and physicochemical wastewater treatment processes reduce the prevalence of virulent *Escherichia coli*. *Appl. Environ. Microbiol.* **2013**, *79* (3), 835−844. Toze, S. PCR and the detection of microbial pathogens in water and wastewater. *Water Res.* **1999**, *33* (17), 3545−3556.
(28) Weinman, S. T.; Fierce, E. M.; Husson, S. M. Nanopatterning commercial nanofiltration and reverse osmosis membranes. *Sep. Purif. Technol.* **2019**, *209*, 646−657.
(29) Dobosz, K. M.; Kuo-Leblanc, C. A.; Bowden, J. W.; Schiffman, J. D. Robust, small diameter hydrophilic nanofibers improve the flux of ultrafiltration membranes. *Ind. Eng. Chem. Res.* **2021**, *60* (25), 9179−9188.
(30) Eren, E.; Sarihan, A.; Eren, B.; Gumus, H.; Kocak, F. O. Preparation, characterization and performance enhancement of polysulfone ultrafiltration membrane using PBI as hydrophilic modifier. *J. Membr. Sci.* **2015**, *475*, 1−8.
(31) Kurtz, I. S.; Sui, S.; Hao, X.; Huang, M.; Perry, S. L.; Schiffman, J. D. Bacteria-resistant, transparent, free-standing films prepared from complex coacervates. *ACS Appl. Bio Mater.* **2019**, *2* (9), 3926−3933.
(32) Rasband, W. S. *ImageJ*; US National Institutes of Health: Bethesda, MA, 2011.
(33) Yang, Z.; Li, L.; Jiang, C.; Zhao, N.; Zhang, S.; Guo, Y.; Chen, Y.; Xue, S.; Ji, C.; Zhao, S.; et al. Tailored thin film nanocomposite membrane incorporated with Noria for simultaneously overcoming the permeability-selectivity trade-off and the membrane fouling in nanofiltration process. *J. Membr. Sci.* **2021**, *640*, 119863. Maggay, I. V. B.; Aini, H. N.; Lagman, M. M. G.; Tang, S.-H.; Aquino, R. R.; Chang, Y.; Venault, A. A biofouling resistant zwitterionic polysulfone

https://doi.org/10.1021/acsestwater.2c00256
ACS EST Water XXXX, XXX, XXX−XXX

membrane prepared by a dual-bath procedure. *Membranes* **2022**, *12* (1), 69. Lin, Y.; Xie, Y.; Chen, F.; Gong, S.; Yang, W.; Liang, X.; Lian, Y.; Chen, J.; Wei, F.; Bai, W.; et al. Bioinspired self-stratification fouling release silicone coating with strong adhesion to substrate. *Chem. Eng. J.* **2022**, *446*, 137043.

(34) Asatekin, A.; Kang, S.; Elimelech, M.; Mayes, A. M. Anti-fouling ultrafiltration membranes containing polyacrylonitrile-graft-poly-(ethylene oxide) comb copolymer additives. *J. Membr. Sci.* **2007**, *298* (1), 136−146. Diagne, F.; Malaisamy, R.; Boddie, V.; Holbrook, R. D.; Eribo, B.; Jones, K. L. Polyelectrolyte and silver nanoparticle modification of microfiltration membranes to mitigate organic and bacterial fouling. *Environ. Sci. Technol.* **2012**, *46* (7), 4025−4033.

(35) Cihanoğlu, A.; Altinkaya, S. A. A facile route to the preparation of antibacterial polysulfone-sulfonated polyethersulfone ultrafiltration membranes using a cationic surfactant cetyltrimethylammonium bromide. *J. Membr. Sci.* **2020**, *594*, 117438.

(36) Kolewe, K. W.; Dobosz, K. M.; Rieger, K. A.; Chang, C.-C.; Emrick, T.; Schiffman, J. D. Antifouling electrospun nanofiber mats functionalized with polymer zwitterions. *ACS Appl. Mater. Interfaces* **2016**, *8* (41), 27585−27593.

(37) Cha, T.-G.; Yi, J. W.; Moon, M.-W.; Lee, K.-R.; Kim, H.-Y. Nanoscale patterning of microtextured surfaces to control super-hydrophobic robustness. *Langmuir* **2010**, *26* (11), 8319−8326. Whyman, G.; Bormashenko, E.; Stein, T. The rigorous derivation of Young, Cassie−Baxter and Wenzel equations and the analysis of the contact angle hysteresis phenomenon. *Chem. Phys. Lett.* **2008**, *450* (4), 355−359.

(38) Tang, C. Y.; Kwon, Y.-N.; Leckie, J. O. Effect of membrane chemistry and coating layer on physiochemical properties of thin film composite polyamide RO and NF membranes: I. FTIR and XPS characterization of polyamide and coating layer chemistry. *Desalination* **2009**, *242* (1), 149−167.

(39) Tang, C. Y.; Kwon, Y.-N.; Leckie, J. O. Probing the nano- and micro-scales of reverse osmosis membranes—A comprehensive characterization of physiochemical properties of uncoated and coated membranes by XPS, TEM, ATR-FTIR, and streaming potential measurements. *J. Membr. Sci.* **2007**, *287* (1), 146−156.

(40) Ma, Z.; Liang, S.; Xiao, K.; Wang, X.; Li, M.; Huang, X. Superhydrophilic polyvinylidene fluoride membrane with hierarchical surface structures fabricated via nanoimprint and nanoparticle grafting. *J. Membr. Sci.* **2020**, *612*, 118332. Hutfles, J.; Chapman, W.; Pellegrino, J. Roll-to-roll nanoimprint lithography of ultrafiltration membrane. *J. Appl. Polym. Sci.* **2018**, *135* (11), 45993.

(41) Khoerunnisa, F.; Nurhayati, M.; Annisa, N. A. A.; Fatimah, S.; Nashrah, N.; Hendrawan, H.; Ko, Y.-G.; Ng, E.-P.; Opaprakasit, P. Effects of benzalkonium chloride contents on structures, properties, and ultrafiltration performances of chitosan-based nanocomposite membranes. *Membranes* **2022**, *12* (3), 268. Shamsuddin, N.; Das, D. B.; Starov, V. M. Filtration of natural organic matter using ultrafiltration membranes for drinking water purposes: Circular cross-flow compared with stirred dead end flow. *Chem. Eng. J.* **2015**, *276*, 331−339. Becht, N. O.; Malik, D. J.; Tarleton, E. S. Evaluation and comparison of protein ultrafiltration test results: Dead-end stirred cell compared with a cross-flow system. *Sep. Purif. Technol.* **2008**, *62* (1), 228−239. Chun, M.-S.; Park, W. C. Time evolution of electrokinetic flow-induced streaming potential and flux in dead-end and cross-flow filtration of colloids through nanopores. *J. Membr. Sci.* **2004**, *243* (1), 417−424.

(42) Heckmann, T. S.; Schiffman, J. D. Spatially organized nanopillar arrays dissimilarly affect the antifouling and antibacterial activities of *Escherichia coli* and *Staphylococcus aureus*. *ACS Appl. Nano Mater.* **2020**, *3* (2), 977−984. Hochbaum, A. I.; Aizenberg, J. Bacteria pattern spontaneously on periodic nanostructure arrays. *Nano Lett.* **2010**, *10* (9), 3717−3721.

(43) Ma, S.; Song, L. Numerical study on permeate flux enhancement by spacers in a crossflow reverse osmosis channel. *J. Membr. Sci.* **2006**, *284* (1), 102−109.

https://doi.org/10.1021/acsestwater.2c00256
ACS EST Water XXXX, XXX, XXX−XXX